Nonclassical State Generation and Quantum Metrology in the Double-Morse Potential

Firoz Chogle , , Berihu Teklu , 1, 2, * Jorge Zubelli , and Ernesto Damiani , 2, 3

¹College of Computing and Mathematical Sciences, Department of Applied Mathematics and Sciences, Khalifa University of Science and Technology, 127788, Abu Dhabi, United Arab Emirates

²Center for Cyber-Physical Systems (C2PS), Khalifa University of Science and Technology, 127788, Abu Dhabi, United Arab Emirates

³Department of Computer Science, University of Milan, Milan, Italy

(Dated: November 12, 2025)

In this paper, we investigate the nonlinear properties of the double-Morse potential as a possible resource for single-mode quantum states because of its double-well structure and anharmonicity. We derive the ground state wave function and the associated energy spectrum analytically, using the asymmetry (width parameter) α as the primary control parameter. These results show a systematic and evident influence on α . We assess the non-Gaussianity and non-classicality measures, quantifying their nonlinearity and quantum behavior. In particular, we discover that both metrics rise monotonically with α . Furthermore, we examine the metrological performance for estimating α . By calculating the pertinent Fisher information and building workable estimators, we show that optimal strategies can saturate the Cramér–Rao bound, with straightforward position measurements on shallow wells already producing high precision. These results collectively demonstrate that the double-Morse potential is a genuine, controllable source of non-Gaussianity, whose non-classicality and metrological applications increase with α . We highlight the potential applications of this model in real-world quantum technologies and discuss the implications for continuous-variable quantum information processing and computation.

I. INTRODUCTION

The quantum technology revolution, in which fundamental physical phenomena such as entanglement and superposition, which do not feature a classical analog, can be harnessed for ground-breaking applications in computation [1], secure communication [2-5], sensing and metrology [6-13] and machine learning [14, 15]. The concept of nonclassicality first attracted significant attention in quantum optics, where quantum states that exhibit genuinely nonclassical characteristics, such as photon antibunching, squeezing, or negativity of quasiprobability distributions, were essential to understanding and utilizing light beyond classical limits. An appropriate platform for exploring nonclassicality, both theoretically and experimentally, has been single-mode radiation fields and, more generally, single-mode bosonic systems. In this context, single-mode bosonic systems provide a natural and experimentally accessible platform for exploring the generation, manipulation, and characterization of nonclassical states. Identifying which quantum features are fundamentally nonclassical and developing rigorous methods to quantify them has thus become a central theme in the theory and application of quantum technologies [16].

In recent decades, single-mode bosonic systems, such as quantized electromagnetic field modes in optical cavities or microwave resonators, have emerged as ideal candidates for the theoretical formulation and experimental investigation of nonclassicality [17–21]. These systems enable precise control over the generation and characterization of quantum features [22–27]. Moreover, nonlinear interaction models accessible through these platforms are experimentally realizable in various oscillatory systems, including mechanical and electromagnetic ones [28, 29]. Nevertheless, a comprehensive understanding of how nonlinearity influences quantumness remains an open and largely unexplored question.

The quantum-to-classical transition in nonlinear nanoelectromechanical systems (NEMS) has been examined in previous studies, including those conducted by Katz et al. [30, 31], which considered both closed and open system dynamics. These investigations examined how quantum signatures appear and are suppressed, particularly as thermal effects increase. Based on this framework, more recent research has started to investigate the structural function of nonlinearity as a tool for producing and maintaining nonclassicality. Teklu et al. [32] specifically studied a Duffing-type nonlinear nanomechanical resonator. They demonstrated that the Wigner function's negativity, a quantitative indicator of nonclassicality, rises with the system's nonlinearity. The idea that nonlinearity might be used to magnify quantum features in bosonic systems was further supported by complementary results in [33], where a broader class of anharmonic potentials was studied. Despite these promising results, a general framework connecting nonlinearity to nonclassicality in the system remains an open research direction, particularly beyond specific models, such as the Duffing oscillator. Motivated by these results, we contribute to this line of inquiry by investigating a quantum double Morse oscillator, aiming to clarify whether such a nonlinear potential can also serve as a platform for enhancing quantum effects in a tunable and structurally generalizable way. Finally, we employ techniques from local quantum estimating theory to characterize the double Morse potential and determine the optimal approach to infer the width parameter [34–38]. In this procedure, the figure of merit is the quantum Fisher information, which quantifies the amount of information about a parameter that can be extracted through measurements performed on a family of quantum states.

This paper is organized as follows: In Section II we introduce the double–Morse (DM) oscillator and fix our notation, derive the exact ground state and its spectrum in dimensionless units, and discuss how the width/asymmetry parameter α controls the potential's nonlinearity. We then define and

^{*} Corresponding author: berihu.gebrehiwot@ku.ac.ae

compute two complementary indicators of "resourcefulness": a Bures-distance-based nonlinearity measure and the relative-entropy non-Gaussianity, and we obtain a closed-form expression for the ground-state Wigner function-written in terms of modified Bessel functions of imaginary order—from which we evaluate Wigner negativity and the associated nonclassicality. We also recall the entanglement potential operational test by interfering the state with the vacuum at a 50:50 beam splitter. Next, in Section III, we cast the estimation of α within local quantum estimation theory, review classical and quantum Fisher information (via the symmetric logarithmic derivative), and derive a compact formula for the QFI of the DM ground state, showing that position measurements saturate the quantum Cramér-Rao bound. Section IV summarizes the main findings and outlines implications for quantum technologies.

II. PRELIMINARIES

This section reviews the primary tools employed in the present work: the concept of the double Morse oscillator, the quantification of nonclassicality of quantum states and nonlinearity of potentials. We begin with an overview of the double Morse potential, followed by a discussion of its relevance in the context of quantum nonlinearity.

A. Double-Morse Oscillator

The Morse potential is commonly used to model the interaction between atoms in a diatomic molecule. It offers a more realistic model than the harmonic oscillator due to its anharmonicity and asymptotic behavior [39]. It is typically expressed as

$$V_{\rm M}(x) = D\left(e^{-2\alpha x} - 2e^{-\alpha x}\right),\tag{1}$$

where D denotes the bond dissociation energy, and the parameter α is responsible for the width of the potential well. The double Morse potential is constructed by superimposing two Morse potentials centered at $\pm x_0$, each facing the other, i.e., with $\pm \alpha$. The resulting expression is

$$V_{\rm DM}(x) = D \left(A \cosh \left(\alpha x \right) - 1 \right)^2, \tag{2}$$

where $A=2e^{-\alpha x_0}$. A constant term resulting from the summation is dropped, as it merely shifts the potential energy by a constant and does not affect the physical behavior of the system. For 0 < A < 1, Eq. (2) describes a symmetric bistable potential with two wells. It is instructive to examine the nonlinear potential-energy landscape that governs the oscillator. As shown in Fig. 1, when D and x_0 are held fixed (so that $A=2e^{-\alpha x_0}$ varies with α), increasing α beyond the threshold $\alpha x_0 = \ln 2$ (i.e., A < 1) transforms the profile from a single, nearly harmonic well into a symmetric double well. The minima move away from the origin toward $\pm x_0$,

so the interwell separation $2|x_{\min}|$ grows from zero and approaches $2x_0$ as $\alpha \to \infty$, while the central barrier height $V(0) = D(1 - 2e^{-\alpha x_0})^2$ rises monotonically toward D.

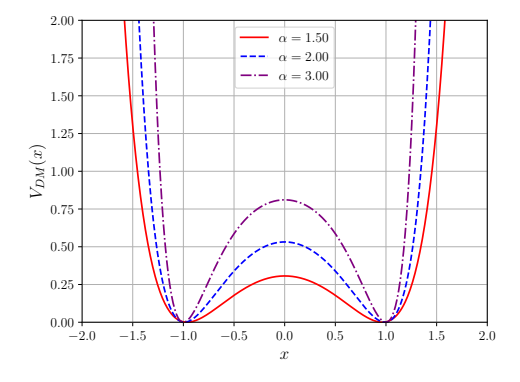


FIG. 1. Double Morse potential profiles for various values of α .

The double Morse potential has been extensively studied over the past four decades [40–52]. It belongs to the class of quasi-exactly solvable (QES) models, for which analytic solutions to the Schrödinger equation exist for specific parameter choices [53]. Alternative forms of QES bistable potentials have been proposed [40–45]. Still, these can be shown to be mathematically equivalent to the double Morse potential under suitable transformations—the solutions to the corresponding Schrödinger equation yield similar eigenfunctions and spectra.

The double Morse potential has been applied in various physical contexts, such as modeling spin systems [45], describing intra-molecular inversion [47], and characterizing the motion and phase transitions of protons in hydrogen-oxygen bonds in ferroelectrics and solids [41, 42, 46]. It has also been used to investigate classical dynamics [49] and chaotic behavior [48]. More recently, quantum wave packet dynamics of the double Morse oscillator have been studied to explore resonance phenomena and wave revivals, with potential applications in quantum information processing and computation [52, 54].

While previous work has used the double Morse potential to model and predict experimental results, the inherent quantum features, particularly its nonclassicality and application to quantum sensing, have not been investigated in depth. Given its anharmonic nature, one can quantify the system's nonlinearity, which is closely linked to nonclassical behavior, by examining its ground state properties [55].

To this end, we consider a single particle of mass m under the influence of the double Morse potential defined in Eq. (2). The position-space wavefunction describes the probability density of finding the particle at a given position $\psi(x)$, which satisfies the time-independent Schrödinger equation:

$$-\frac{\hbar^2}{2m}\frac{\partial^2 \psi(x)}{\partial x^2} + D(A\cosh(\alpha x) - 1)^2 \psi(x) = E\psi(x) \quad (3)$$

where E is the energy eigenvalue of the particle corresponding to the state $\psi(x)$. To simplify the analysis, we adopt dimensionless variables such that distances and energies are measured

in units of $1/\alpha$ and $\hbar^2\alpha^2/(2m)$, respectively. Following the approach in Ref. [43], Eq. (3) is non-dimensionalized by introducing the following transformations

$$\alpha x = 2y, \; \mu^2 = \frac{8mD}{\hbar^2 \alpha^2}, \; \text{and} \; \epsilon = \frac{8mE}{\hbar^2 \alpha^2}.$$

The Schrödinger equation in these new units becomes

$$\frac{d^2\psi}{dy^2} + [\epsilon - \mu^2 (A\cosh 2y - 1)^2]\psi = 0.$$
 (4)

The bound-state solutions of Eq. (4) vanish asymptotically, i.e., $\psi(y) \to 0$ as $y \to \pm \infty$. This leads to the following proposition:

Proposition 1. The asymptotic solution of Eq. (4) as $y \to \pm \infty$ is given by

$$\psi(y) \approx \exp\left(-\frac{\mu A}{2}\cosh 2y\right)$$
 (5)

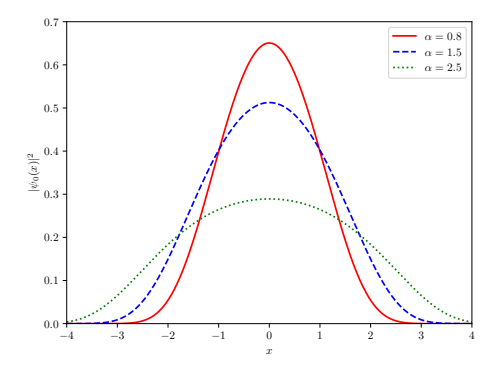


FIG. 2. Ground-state probability density $|\psi_0(x)|^2$ of the double-Morse oscillator for several values of α . Increasing α narrows the distribution in x and enhances localization at the well minima.

Building on Proposition 1, the general wavefunction can be expressed as $\psi(y)=\exp\left(-\frac{\mu A}{2}\cosh 2y\right)\phi(y)$, where $\phi(y)$ satisfies the differential equation:

$$\frac{d^2\phi}{dy^2} - 2A\mu \sinh 2y \frac{d\phi}{dy} + (\tilde{\epsilon} + 2\mu A(\mu - 1)\cosh 2y)\phi = 0.$$
 (6)

with $\tilde{\epsilon} = \epsilon - \mu^2 (1 + A^2)$. When $\mu = n + 1$, the function $\phi(y)$ becomes a polynomial in hyperbolic functions, allowing the system to support n+1 bound states. The recurrence relations for the polynomial coefficients are obtained from Eq. (6), and the condition for non-trivial polynomial solutions is that the determinant of the associated coefficient matrix vanishes. The roots of this determinant equation yield the allowed energy levels.

Since our analysis focuses on the ground state, Eq. (6) is solved for n=0. The ground-state wavefunction is given by

$$\psi_0(y) = \frac{1}{\sqrt{K_0(A)}} \exp\left(-\frac{A}{2}\cosh 2y\right) \tag{7}$$

where $K_0(A)$ is the zeroth-order modified Bessel function of the second kind. The corresponding ground-state energy is $\epsilon_0 = \mu^2 (1 + A^2)$.

The nonlinearity of the potential is controlled by the parameter α . For a bistable configuration, the condition $0 < A = 2e^{-\alpha x_0} < 1$ must hold, leading to the constraint

$$\frac{\ln 2}{x_0} < \alpha < \infty.$$

Intuitively, larger values of α correspond to a higher degree of nonlinearity.

Figure 2 shows the ground-state probability density $|\psi_0(x)|^2$ of the double-Morse oscillator for several values of α . As α increases, the density narrows in x and becomes more localized around the well minima, with a correspondingly deeper dip between the wells. As we demonstrate, the ground-state wave function plays a central role in the analysis presented in this work. We now turn to probing the nonlinear features of the system using ground-state properties.

B. Probing the nonlinear features of a one-dimensional potential using ground states

We begin by introducing a measure of nonlinearity that relies on the properties of the ground state (GS) [55] and is constructed by comparing the perturbed ground state $|\psi_0\rangle$ with its unperturbed harmonic counterpart $|0\rangle$. Specifically, we quantify the distance between these two ground states using the Bures metric. For a perturbing nonlinear potential $\hat{V}(\hat{x})$, the nonlinearity measure $\eta_B[V]$ is defined as the appropriately normalized Bures distance \mathcal{D}_B between the ground state of the oscillator under consideration and that of the corresponding harmonic oscillator. In this case, we have

$$\eta_{\rm B}[V] = \frac{1}{\sqrt{2}} \mathcal{D}_{\rm B}\left[|\psi_0\rangle_V, |0\rangle_H\right] \tag{8}$$

where $|0\rangle_H$ is the GS of the reference QHO. Although this measure is intuitively appealing, identifying a suitable reference QHO potential for a given system is not always feasible. The non-Gaussianity of the GS is one of the most peculiar features of a nonlinear oscillator, since it is apparent that the more the oscillator is similar to the harmonic one, the more the GS has a wave-function similar to a Gaussian. So, it is quite natural to use a bona-fide measure of non-Gaussianity for the GS to quantify the nonlinearity. In [56, 57], a more robust measure of non-Gaussianity was introduced, which did not involve finding a reference potential. This approach evaluates the quantum relative entropy between the state under consideration and its reference Gaussian state. The main properties of this measure and its extension to pure states are discussed in [55]. For the GS of a given potential, the non-Gaussianity measure takes the form

$$\eta_{\rm NG}[V] = h\left(\sqrt{\det\sigma}\right)$$
(9)

where σ is the covariance matrix of the GS and the function $h(x) = \left(x + \frac{1}{2}\right) \ln\left(x + \frac{1}{2}\right) - \left(x - \frac{1}{2}\right) \ln\left(x - \frac{1}{2}\right)$. The covariance variance matrix calculated with the state (7) is the following:

$$\sigma = \begin{pmatrix} \langle \hat{x}^2 \rangle - \langle \hat{x} \rangle^2 & \frac{1}{2} \langle \{\hat{x}, \hat{p}\} \rangle - \langle \hat{x} \rangle \langle \hat{p} \rangle \\ \frac{1}{2} \langle \{\hat{p}, \hat{x}\} \rangle - \langle \hat{p} \rangle \langle \hat{x} \rangle & \langle \hat{p}^2 \rangle - \langle \hat{p} \rangle^2 \end{pmatrix}.$$

where $\{\cdot,\cdot\}$ denotes the anti-commutator and $[\hat{x},\hat{p}]=i$. The diagonal entries are the variances of \hat{x} and \hat{p} ; symmetry implies $\sigma_{12}=\sigma_{21}$ (See Appendix A).

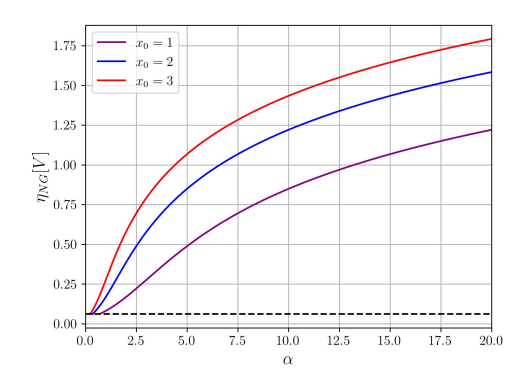


FIG. 3. Non-Gaussianity measure as a function of α for values of $x_0=1,2$ and 3. The dashed black line is $\eta_{\text{NG}[V]}\approx 0.0615$.

Fig (3) shows the non-Gaussianity measure $\eta_{\rm NG}$ versus α . As α increases, the ground state becomes more strongly non-Gaussian. The curves for different well separations x_0 illustrate that a larger x_0 (i.e., more widely separated minima) yields a more non-Gaussian ground state. To retain a double-well, we require $\alpha \in ((\ln 2)/x_0, \infty)$.

The covariance-matrix elements depend on a parameter $A(\alpha,x_0)$. For $\alpha\approx(\ln 2)/x_0$, we have $A\approx 1$ (independent of x_0), so $\eta_{\rm NG}$ starts at the common value ≈ 0.0615 , indicated by the dashed line in Fig (3). In the opposite limit, $\alpha\to\infty$ implies $A\to 0$, the covariance-matrix elements grow without bound, and the x_0 -dependence disappears; consequently, the $\eta_{\rm NG}$ curves merge for $\alpha\gg 1$.

C. Nonclassicality measure

An alternate way to quantify the "quantumness" of a state is to assess its deviation from a classical description via its phase-space representation, particularly the Wigner distribution. Introduced to study quantum corrections to statistical mechanics [58–60], the Wigner distribution of a state ρ is

$$W(x,p) = \frac{1}{\pi\hbar} \int_{-\infty}^{+\infty} \langle x + y | \rho | x - y \rangle e^{-2ipy/\hbar} \, \mathrm{d}y. \quad (10)$$

For pure states, Hudson's theorem asserts that W(x, p) is everywhere non-negative if and only if the state is Gaussian [61]. Equivalently, any *non-Gaussian* pure state necessarily exhibits

Wigner negativity. Because of these negative regions, W is a $\it quasi$ probability distribution rather than a true probability density.

A common way to quantify the negativity is via

$$\nu \equiv \int_{-\infty}^{+\infty} \int_{-\infty}^{+\infty} \left| W(x, p) \right| \mathrm{d}x \, \mathrm{d}p - 1, \tag{11}$$

which equals twice the integrated negative "volume," i.e. $\nu=2\int_{W<0}|W(x,p)|\,\mathrm{d}x\,\mathrm{d}p$. Following [62], we define the (bounded) non-classicality measure

$$\eta_{\rm NC} = \frac{\nu}{\nu + 1}.\tag{12}$$

This measure vanishes for states with non-negative Wigner functions (e.g., pure Gaussian states). Note that (12) is most meaningful for *pure* states: Wigner positivity does not imply Gaussianity or classicality for mixed states. For example, incoherent mixtures of coherent states ("decohered" Schrödingercat states) can have a positive Wigner distribution while remaining non-Gaussian [63].

Using (10), the Wigner distribution of the ground state is

$$W_0(x,p) = \frac{1}{\pi K_0(A)} \int_0^\infty e^{-A \cosh(2x) \cosh y} \cos(py) \, dy,$$
(13)

which can be evaluated in closed form by writing $\cos(py) = \cosh(ipy)$ and using the integral representation of the modified Bessel function [64],

$$K_{\nu}(z) = \int_0^\infty e^{-z \cosh t} \cosh(\nu t) dt. \tag{14}$$

This yields

$$W_0(x,p) = \frac{1}{\pi K_0(A)} K_{ip}(A\cosh(2x)).$$
 (15)

Here K_{ip} is the modified Bessel function of the second kind (also called "third kind") with purely imaginary order [65–68]. Although numerics are typically used to evaluate K_{ip} , several properties are immediate: (i) for $p \in \mathbb{R}$ and A>0 (doublewell regime), since $\cosh(2x)>0$ for all x, the argument $A\cosh(2x)$ is positive and hence $K_{ip}(A\cosh(2x))\in\mathbb{R}$. (ii) $K_{-ip}=K_{ip}$, so W_0 is even in p. (iii) the Wigner function is normalized,

$$\iint W_0(x,p) \, \mathrm{d}x \, \mathrm{d}p = 1.$$

Substituting the explicit form of W_0 yields the identity

$$\iint K_{ip}(A\cosh(2x)) dx dp = \pi K_0(A).$$

Figure 4 shows $W_0(x,p)$ for $\alpha=5$ and $x_0=1$. The Wigner function exhibits regions where $W_0<0$, a hallmark of nonclassicality for pure states. In a double-well potential, these negative regions arise from quantum interference between the two components of the ground-state wavefunction

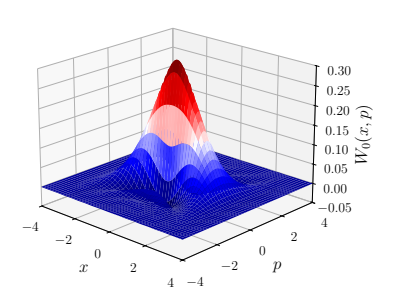


FIG. 4. (Color online) Ground-state Wigner distribution $W_0(x,p)$ for $\alpha=5$ and $x_0=1$. Surface height equals $W_0(x,p)$; red (blue) shading indicates positive (negative) values. Axes are dimensionless and W_0 is normalized so that $\int \int W_0 \, \mathrm{d}x \, \mathrm{d}p = 1$. The appearance of negative-valued regions provides a direct signature of nonclassicality for a pure state. For animations of the Wigner function, see here.

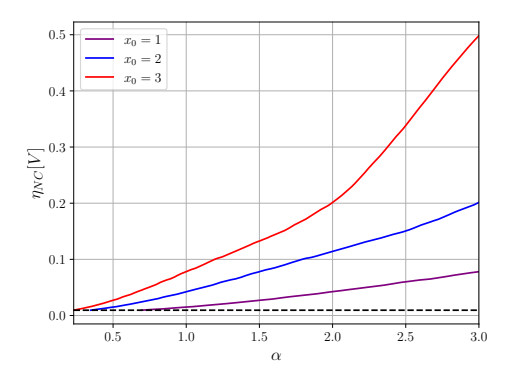


FIG. 5. Nonclassicality measure $\eta_{\rm NC}$ as a function of α for the ground state with $x_0=1,2,3$. The dashed line marks $\eta_{\rm NC}\approx 0.009$.

that delocalize across the central barrier. In phase space, this interference appears as oscillatory fringes—alternating positive and negative bands—most prominently near the barrier region (moderate x) and along the momentum direction; within each well, where the state locally resembles a Gaussian packet, W_0 is predominantly positive. The pattern is even in both x and p (since $\cosh 2x$ is even and $K_{-ip}=K_{ip}$), which underlies the quadrant reduction used to compute the integrated negativity:

$$\nu = \frac{4}{\pi K_0(A)} \int_0^\infty \mathrm{d}x \int_0^\infty \mathrm{d}p \left| K_{ip} (A \cosh(2x)) \right| - 1.$$
(16)

Using Eqs. (12) and (16), we evaluate the nonclassicality $\eta_{\rm NC}$. As shown in Fig. 5, $\eta_{\rm NC}$ rises monotonically with α for $x_0=1,2,3$, indicating that the ground state becomes increasingly nonclassical as the double well deepens and separates. In the shallow-well regime $\alpha \approx (\ln 2)/x_0$, all curves start from the same small baseline $\eta_{\rm NC} \approx 0.009$ (dashed reference), consistent with a nearly Gaussian ground state with negligible Wigner negativity. Increasing α enhances interference between

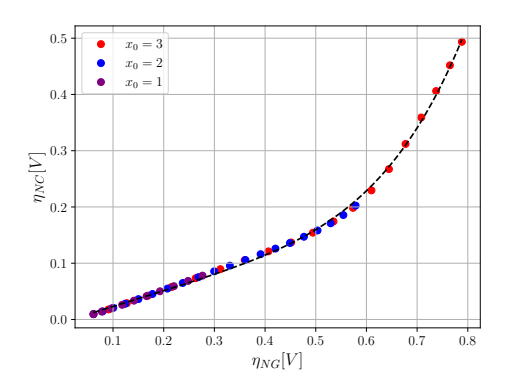


FIG. 6. Parametric relation between non-Gaussianity $\eta_{\rm NG}$ and non-classicality $\eta_{\rm NC}$. Symbols denote different x_0 ; the dashed curve is the fit to Eq. (17).

the two localized components, which increases the integrated negativity ν and the nonclassicality $\eta_{\rm NC}$.

To quantify how non-Gaussianity and nonclassicality covary, we plot $\eta_{\rm NC}$ versus $\eta_{\rm NG}$ in Fig. 6. Data for $x_0=1,2,3$ collapse onto a single monotone curve: the dependence is approximately linear for small $\eta_{\rm NG}$ and becomes superlinear at larger $\eta_{\rm NG}$. We model this behavior with

$$\eta_{\rm NC} = a + b \, \eta_{\rm NG} + \eta_{\rm NG}^{\,c},\tag{17}$$

which captures both the near-linear onset and the faster growth at higher non-Gaussianity. A least-squares fit yields

$$a = (-4.73 \times 10^{-3}) \pm (0.04 \times 10^{-3})$$

$$b = 0.28 \pm (0.18 \times 10^{-5})$$

$$c = 5.31 \pm (0.17 \times 10^{-3}).$$

The small, slightly negative intercept a lies within systematic/numerical uncertainty and is consistent with the expectation that $\eta_{\rm NC} \to 0$ as $\eta_{\rm NG} \to 0$ (Gaussian limit).

D. Entanglement potential

In quantum optics, a single—mode state is considered nonclassical if, after passage through a passive linear—optical device, it can generate bipartite entanglement between two output modes. An operational quantifier of this resource is the *entanglement potential* (EP): the entanglement created when the state interferes with the vacuum at a beam splitter [69–71]. It is sufficient and optimal to consider a lossless 50:50 beam splitter with vacuum in the auxiliary port; additional passive optics or extra vacuum ancillas cannot increase the bipartite entanglement across the output partition [71]. Related experimental and theoretical refinements appear in Refs. [72, 73].

Let $|\psi\rangle$ be the input single–mode pure state and $|0\rangle$ the vacuum in the auxiliary input. The joint input is

$$|\Psi_{\rm in}\rangle = |\psi\rangle \otimes |0\rangle. \tag{18}$$

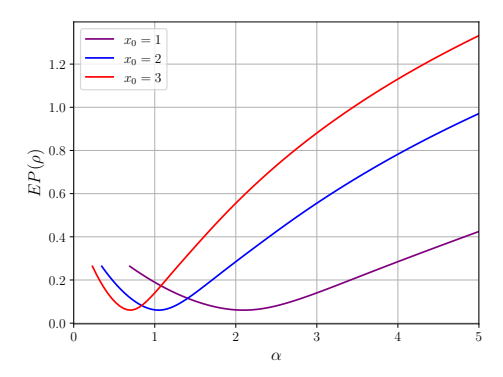


FIG. 7. Entanglement potential $EP(\rho)$ generated by a 50:50 beam splitter as a function of the state parameter α . Three curves, labeled by $x_0 \in \{1,2,3\}$, show how this model parameter influences both the scale and the α -dependence of the output entanglement. As expected, $EP(\rho)=0$ at $\alpha=0$ (vacuum), while nonzero α yields finite two-mode entanglement at the output.

The beam-splitter unitary can be written as

$$\hat{U}(\xi) = \exp(\xi \,\hat{a}^{\dagger} \hat{b} - \xi^* \,\hat{a} \hat{b}^{\dagger}), \qquad \xi = \phi \,e^{i\theta}, \quad (19)$$

with \hat{a} (\hat{b}) acting on output mode A (B). Using Schwinger's two–mode boson representation of SU(2), one obtains the disentangled form

$$\hat{U}(\xi) = \exp\left[-e^{i\theta} \tan\phi \,\hat{a}\hat{b}^{\dagger}\right] (\cos\phi)^{\hat{a}^{\dagger}\hat{a} - \hat{b}^{\dagger}\hat{b}} \,\exp\left[e^{i\theta} \tan\phi \,\hat{a}^{\dagger}\hat{b}\right]. \tag{20}$$

A 50:50 splitter corresponds to $\phi = \pi/4$; we denote $\hat{B} \equiv \hat{U}(\pi/4)$. The output state is then

$$|\Psi_{\text{out}}\rangle = \hat{B} |\Psi_{\text{in}}\rangle.$$
 (21)

For pure inputs, the EP reduces to the von Neumann entropy of either reduced state,

$$E[\rho] = -\text{Tr}_B[\rho_B \log \rho_B] = -\text{Tr}_A[\rho_A \log \rho_A], \quad (22)$$

with $\rho = |\Psi_{\text{out}}\rangle\langle\Psi_{\text{out}}|$, $\rho_A = \text{Tr}_B[\rho]$, and $\rho_B = \text{Tr}_A[\rho]$. Equivalently,

$$E[\rho] = E[\hat{B}(|\psi\rangle\langle\psi| \otimes |0\rangle\langle0|) \hat{B}^{\dagger}]. \tag{23}$$

Figure 7 shows the entanglement potential $EP(\rho)$ as a function of the width parameter α for three values of x_0 . Across the full range $\alpha \in [0,5]$, $EP(\rho)$ increases monotonically from near zero and gradually approaches a shallow plateau (with the fastest rise for small α). Larger x_0 yields a uniformly higher entanglement at fixed α , the curves satisfy $x_0{=}3>2>1$ over the entire domain, while their separation diminishes as α grows and the curves level off. No nonmonotonic features are observed, indicating that broadening the potential (increasing α) enhances the output two–mode entanglement up to a saturation regime.

III. LOCAL QUANTUM ESTIMATION

Quantum technologies rely on properties of individual quantum systems and can often outperform any conventional technology in precision measurements and information processing. Relevant examples may be found in quantum metrology, which allows one to achieve much more sensitive parameter estimation than any conventional techniques. Indeed, quantum properties of physical systems are *fragile* to decoherence, which in turn makes suitably engineered sensors exceptionally sensitive to small parameter changes.

Local quantum estimation theory (QET) looks for the measurement maximizing the Fisher information, an abstract quantity that measures the maximum information about the parameter we wish to estimate from a given measurement procedure, thus minimizing the variance of the estimator. Roughly speaking, one may expect local QET to provide better performances since the optimization concerns a specific value of the parameter, with some adaptive or feedback mechanism assuring the achievability of the ultimate bound.

Local QET has been successfully applied to estimation problems in open quantum systems, non-unitary processes and nonlinear quantities as entanglement [36, 74–87] and for a closed system, evolving under a unitary transformation [88]. The geometric structure of QET has been exploited to assess quantum criticality as a resource for quantum estimation [89].

A. Quantum Fisher information

In classical estimation theory, a family of distributions $p(x|\theta)$ has classical Fisher information (CFI)

$$F_{\theta} = \int p(x|\theta) \left(\frac{\partial}{\partial \theta} \log p(x|\theta)\right)^{2} dx \tag{24}$$

$$= \int \frac{1}{p(x|\theta)} \left(\frac{\partial p(x|\theta)}{\partial \theta}\right)^2 dx, \tag{25}$$

and any unbiased estimator $\hat{\theta}$ obeys the Cramér-Rao bound

$$\operatorname{Var}(\hat{\theta}) \ge \frac{1}{F_{\theta}}.\tag{26}$$

In the quantum setting, the parameter θ is encoded in a state ρ_{θ} . The symmetric logarithmic derivative (SLD) L_{θ} is defined implicitly by [34, 36]

$$\partial_{\theta} \rho_{\theta} = \frac{1}{2} \left(L_{\theta} \rho_{\theta} + \rho_{\theta} L_{\theta} \right). \tag{27}$$

The quantum Fisher information (QFI) is

$$\mathcal{F}(\theta) = \text{Tr}\left[\rho_{\theta} L_{\theta}^{2}\right], \tag{28}$$

and the quantum Cramér–Rao bound (QCRB) implies that for any (locally) unbiased estimator $\hat{\theta}$,

$$\operatorname{Var}(\hat{\theta}) \ge \frac{1}{\mathcal{F}(\theta)}.$$
 (29)

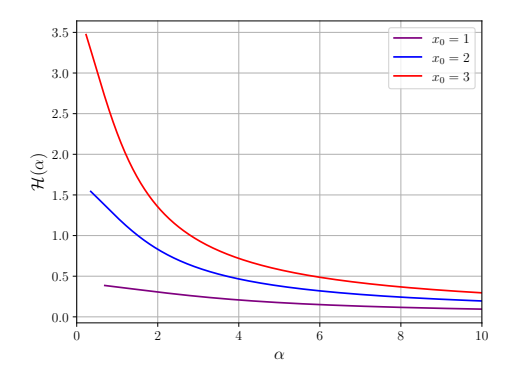


FIG. 8. Fisher information of the ground state wavefunction as a function of α for different values of x_0 .

By writing the quantum state with the spectral decomposition, $\rho_{\theta}=\sum_{n}p_{n}|\psi_{n}\rangle\langle\psi_{n}|$, a widely used expression for the QFI is

$$F(\rho_{\theta}) = \sum_{n} \frac{(\partial_{\theta} p_{n})^{2}}{p_{n}} + \sum_{n} 4p_{n} \langle \partial_{\theta} \psi_{n} \mid \partial_{\theta} \psi_{n} \rangle$$
 (30)

$$-\sum_{m,n} \frac{8p_m p_n}{p_m + p_n} \left| \left\langle \partial_{\theta} \psi_m \mid \psi_n \right\rangle \right|^2. \tag{31}$$

In the case of a pure state $|\psi_{\theta}\rangle$, the above expression further simplifies to [36]

$$\mathcal{F}_{\theta} = 4 \left(\left\langle \partial_{\theta} \psi_{\theta} \mid \partial_{\theta} \psi_{\theta} \right\rangle - \left| \left\langle \psi_{\theta} \mid \partial_{\theta} \psi_{\theta} \right\rangle \right|^{2} \right). \tag{32}$$

Furthermore, note that the real part of $\langle \partial_{\theta} \psi_{\theta} \mid \psi_{\theta} \rangle$ is zero for real states, hence the QFI is just given by

$$\mathcal{F}_{\theta} = 4\langle \partial_{\theta} \psi_{\theta} \mid \partial_{\theta} \psi_{\theta} \rangle. \tag{33}$$

In our model, the straightforward evaluation of the QFI of the ground state wavefunction gives

$$\mathcal{F}(\alpha) = \left(\frac{Ax_0}{K_0(A)}\right)^2 \left[\frac{K_2(A)K_0(A) + K_0^2(A)}{2} - K_1^2(A)\right]. \tag{34}$$

The expression of the quantum Fisher information coincides with the classical one because the ground state wavefunction is a pure and real state. Because the ground state is pure, the optimal measurement can saturate the QCRB, and the (measurement-optimized) classical FI coincides with $\mathcal{F}(\alpha)$.

As shown in Fig. 8, the quantum Fisher information (QFI) of the ground state $\psi_{\alpha}(x)$, denoted $\mathcal{F}(\alpha)$, decreases with α for all well separations $x_0 \in \{1,2,3\}$. This monotonic decrease reflects a diminishing sensitivity of the state to changes in α and, via the quantum Cramér–Rao bound, implies that the minimum achievable variance of any locally unbiased estimator increases as α grows, i.e., $\operatorname{Var}(\hat{\alpha}) \geq [\mathcal{F}(\alpha)]^{-1}$. Conversely, in the shallow-well regime (small α) the QFI is larger, yielding tighter lower bounds on the estimation error of the estimator $\hat{\alpha}$. In this model, the Fisher information associated with position

measurements coincides with the QFI, indicating that position measurements are optimal and exhaust the information available about α for the double Morse oscillators.

IV. CONCLUSION

In this work, we have addressed that the double Morse potential provides a practical and controllable platform for creating non-Gaussian quantum states. The Wigner-function negativities show that when the asymmetry (width parameter) α is tuned, the ground state significantly deviates from Gaussianity and acquires prominent nonclassical properties. Ouantitative measures of non-Gaussianity and non-classicality exhibit a monotonic relationship with each other over the examined parameter regimes, establishing an operational connection between these two resources in this model. The same control parameter also governs the state's capacity to generate bipartite entanglement at a passive 50:50 beam splitter: the entanglement potential $EP(\rho)$ grows with α . It approaches a gentle saturation, with larger x_0 yielding uniformly higher output entanglement (Fig. 7). No non-monotonic behavior is observed, indicating a broad and simple control landscape in which increased structural asymmetry reliably enhances the accessible nonclassical resources.

To estimate the structural parameter α , we examined both metrological performance and state characterization. We found that basic position measurements on the ground state of a shallow well already achieve great precision, and we developed estimators that saturate the Cramér–Rao bound. This finding implies that double-Morse platforms are appealing for quantum sensing tasks related to molecular structure or potential shape recognition, as they can combine creative state construction with experimentally achievable outcomes.

Our findings provide several specific suggestions for further implementation and a broader impact. Tolerances to decoherence and control flaws will first be made clear by evaluating the resilience of the reported non-Gaussianity and Wigner negativities under actual experimental settings, such as weak optical coupling approximated as a harmonic perturbation. Second, by incorporating the entanglement potential [71] into the current nonlinearity witnesses, it is possible to verify that these states are capable of producing entanglement through linear optics, thereby expanding the analysis to mixed states beyond the scope of Hudson's theorem. When implemented together, these approaches make the double Morse oscillator a viable and tunable source of non-Gaussianity for precision metrology [38, 90] and quantum simulation, while the resulting dynamics offer insight into matter-wave packet control and potential applications in quantum information processing and computing [52, 91–96].

ACKNOWLEDGEMENT

This work has been supported by Khalifa University of Science and Technology through the project 8474000739 (RIG-

2024-033).

Appendix A: Covariance Matrix

Non-Gaussianity of the quantum state $\psi(x)$ is measured by considering a reference Gaussian state that has the same mean vector and covariance matrix as $\psi(x)$. The covariance matrix is

$$\sigma = \begin{pmatrix} \langle \hat{x}^2 \rangle - \langle \hat{x} \rangle^2 & \frac{1}{2} \langle \{\hat{x}, \hat{p}\} \rangle - \langle \hat{x} \rangle \langle \hat{p} \rangle \\ \frac{1}{2} \langle \{\hat{p}, \hat{x}\} \rangle - \langle \hat{p} \rangle \langle \hat{x} \rangle & \langle \hat{p}^2 \rangle - \langle \hat{p} \rangle^2 \end{pmatrix}.$$

The operators in the position representation are

$$\hat{x} = x,$$

$$\hat{p} = -i \frac{\partial}{\partial x}.$$

Using $\langle \hat{O} \rangle = \langle \psi_0 | \hat{O} | \psi_0 \rangle = \int_{-\infty}^{+\infty} \psi_0^*(x) \hat{O}_x \psi_0(x) \; dx$, the following expressions are obtained:

$$\langle \hat{x} \rangle = \frac{1}{K_0(A)} \int_{-\infty}^{+\infty} e^{-A \cosh 2x} x \, dx = 0, \tag{A1}$$

$$\langle \hat{p} \rangle = \frac{-Ai}{K_0(A)} \int_{-\infty}^{+\infty} e^{-A\cosh 2x} \sinh 2x \, dx = 0, \tag{A2}$$

$$\langle \hat{x}^2 \rangle = \frac{1}{K_0(A)} \int_{-\infty}^{+\infty} x^2 e^{-A \cosh 2x} dx$$
$$= \frac{1}{4K_0(A)} \int_0^{\infty} y^2 e^{-A \cosh y} dy, \tag{A3}$$

$$\langle \hat{p}^2 \rangle = \frac{A}{K_0(A)} \int_{-\infty}^{+\infty} e^{-A \cosh 2x} \left(2 \cosh 2x - A \sinh^2 2x \right) dx$$
$$= 2A \frac{K_1(A)}{K_0(A)} - \frac{A^2}{2K_0(A)} (K_2(A) - K_0(A)) . \tag{A4}$$

Equations (A1) and (A2) vanish because their integrands are odd. The expression for $\langle \hat{p}^2 \rangle$ follows from Eq. (14). Using the canonical commutation relation $[\hat{x},\hat{p}]=i$, the anti-commutator simplifies to $\{\hat{x},\hat{p}\}=2\hat{x}\hat{p}-i$. Its expectation value is

$$\begin{aligned}
\langle \{\hat{x}, \hat{p}\} \rangle &= \langle 2\hat{x}\hat{p} - i \rangle \\
&= 2\langle \hat{x}\hat{p} \rangle - i \\
&= \frac{2Ai}{K_0(A)} \int_{-\infty}^{+\infty} e^{-A\cosh 2x} x \sinh 2x \, dx - i \\
&= \frac{Ai}{K_0(A)} \int_0^{\infty} e^{-A\cosh y} y \sinh y \, dy - i. \quad (A5)
\end{aligned}$$

The expressions in Eqs. (A3) and (A5) follow from the substitution y=2x. Although these integrals may be evaluated numerically (e.g., by Gauss-Legendre quadrature), it is preferable to obtain analytic forms using Feynman's trick (differentiation under the integral sign). Consider

$$I(b) = \int_0^\infty e^{-A\cosh(bx)} dx.$$
 (A6)

Differentiating with respect to b gives

$$\frac{dI}{db} = -A \int_0^\infty e^{-A\cosh(bx)} \sinh(bx) x \, dx. \tag{A7}$$

Setting b = 1 yields

$$\int_0^\infty e^{-A\cosh x} x \sinh x \, dx = -\frac{1}{A} \left. \frac{dI}{db} \right|_{b=1}. \tag{A8}$$

Using Eq. (A11) to evaluate I(b), one finds

$$\int_0^\infty e^{-A\cosh x} x \sinh x \, dx = \frac{K_0(A)}{A}.$$
 (A9)

Substituting Eq. (A9) into Eq. (A5) gives

$$\langle \{\hat{x}, \hat{p}\} \rangle = 0. \tag{A10}$$

Since the modified Bessel function of the second kind admits the integral representation

$$K_{\nu}(x) = \int_{0}^{\infty} e^{-x \cosh t} \cosh(\nu t) dt.$$
 (A11)

Differentiating Eq. (A11) twice with respect to ν gives

$$\frac{\partial^2 K_{\nu}(x)}{\partial \nu^2} = \int_0^\infty t^2 e^{-x \cosh t} \cosh(\nu t) dt. \tag{A12}$$

For $\nu = 0$ and x = A, the integral on the right coincides with that in Eq. (A3), and therefore

$$\langle \hat{x}^2 \rangle = \frac{1}{4K_0(A)} \left. \frac{\partial^2 K_\nu(A)}{\partial \nu^2} \right|_{\nu=0}.$$
 (A13)

Equation (A13) involves a derivative of K_{ν} with respect to its order rather than its argument; while closed-form expressions are not standard in the literature, this representation is well suited to stable numerical evaluation (or, alternatively, one may compute σ_{11} via Gauss–Legendre quadrature).

The use of differentiation under the integral sign is justified by Lebesgue's dominated convergence theorem [97].

Farid Shahandeh, Austin P. Lund, and Timothy C. Ralph. *Phys. Rev. A*, 99(5):052303, 2019.

^[2] Charles H. Bennett and Gilles Brassard. Quantum cryptography: Public key distribution and coin tossing. In *Proceedings of IEEE*

International Conference on Computers, Systems and Signal Processing, volume 175, pages 7–11, 1984.

^[3] Artur K. Ekert. Phys. Rev. Lett., 67(6):661–663, 1991.

^[4] Charles H. Bennett and Stephen J. Wiesner. Phys. Rev. Lett.,

- 69(20):2881-2884, 1992.
- [5] Carlton M. Caves and Peter D. Drummond. Rev. Mod. Phys., 66(2):481–537, 1994.
- [6] Horace P. Yuen and Masanao Ozawa. Phys. Rev. Lett., 70(4):363–366, 1993.
- [7] G. Mauro D'Ariano, Paoloplacido Lo Presti, and Matteo G. A. Paris. *Phys. Rev. Lett.*, 87(27):270404, 2001.
- [8] Berihu Teklu, Stefano Olivares, and Matteo G. A. Paris. J. Phys. B: At. Mol. Opt. Phys., 42(3):035502, 2009.
- [9] C. F. Ockeloen-Korppi, E. Damskägg, G. S. Paraoanu, F. Massel, and M. A. Sillanpää. *Phys. Rev. Lett.*, 121(24):243601, 2018.
- [10] Alessandro Candeloro, Sholeh Razavian, Matteo Piccolini, Berihu Teklu, Stefano Olivares, and Matteo G. A. Paris. *Entropy*, 23(10), 2021.
- [11] Muhammad Asjad, Berihu Teklu, and Matteo G. A. Paris. *Phys. Rev. Res.*, 5(1):013185, 2023.
- [12] Dong Xie, Chunling Xu, Xiwei Yao, and An Min Wang. Results in Physics, 50:106575, 2023.
- [13] Jiahao Huang, Min Zhuang, and Chaohong Lee. Appl. Phys. Rev., 11:031302, 2024.
- [14] Valeria Cimini, Emanuele Polino, Mauro Valeri, Ilaria Gianani, Nicolò Spagnolo, Giacomo Corrielli, Andrea Crespi, Roberto Osellame, Marco Barbieri, and Fabio Sciarrino. *Phys. Rev. Appl.*, 15(4):044003, 2021.
- [15] Ilaria Gianani, Ivana Mastroserio, Lorenzo Buffoni, Natalia Bruno, Ludovica Donati, Valeria Cimini, Marco Barbieri, Francesco S. Cataliotti, and Filippo Caruso. Adv. Quantum Technol., 5(8):2100140, 2022.
- [16] A. I. Lvovsky. Squeezed light. In *Photonics Volume 1: Fundamentals of Photonics and Physics*, pages 121–164. Wiley, 2015.
- [17] D. Leibfried, R. Blatt, C. Monroe, and D. Wineland. *Rev. Mod. Phys.*, 75(1):281–324, 2003.
- [18] Markus Aspelmeyer, Tobias J. Kippenberg, and Florian Marquardt. Rev. Mod. Phys., 86(4):1391–1452, 2014.
- [19] M. Lewenstein, A. Sanpera, and V. Ahufinger. *Ultracold Atoms in Optical Lattices: Simulating Quantum Many-Body Systems*. Oxford University Press, 2012.
- [20] Benjamin Rogers, Nicola Lo Gullo, Gabriele De Chiara, G. Massimo Palma, and Mauro Paternostro. Hybrid optomechanics for Quantum Technologies. *Quantum Measurements and Quantum Metrology*, 2(1):11–43, 2014.
- [21] A Smirne, T Nitsche, D Egloff, S Barkhofen, S De, I Dhand, C Silberhorn, S F Huelga, and M B Plenio. Experimental control of the degree of non-classicality via quantum coherence. *Quantum Science and Technology*, 5(4):04LT01, jul 2020.
- [22] V Peano and M Thorwart. New J. Phys., 8(2):21, 2006.
- [23] F. R. Ong, M. Boissonneault, F. Mallet, A. Palacios-Laloy, A. Dewes, A. C. Doherty, A. Blais, P. Bertet, D. Vion, and D. Esteve. *Phys. Rev. Lett.*, 106(16):167002, 2011.
- [24] David P DiVincenzo and John A Smolin. New J. Phys., 14(1):013051, 2012.
- [25] Simon Rips and Michael J. Hartmann. Phys. Rev. Lett., 110(12):120503, 2013.
- [26] G. Vacanti, M. Paternostro, G. M. Palma, M. S. Kim, and V. Vedral. *Phys. Rev. A*, 88(1):013851, 2013.
- [27] Víctor Montenegro, Alessandro Ferraro, and Sougato Bose. *Phys. Rev. A*, 90(1):013829, 2014.
- [28] J P Home, D Hanneke, J D Jost, D Leibfried, and D J Wineland. New J. Phys., 13(7):073026, 2011.
- [29] J. C. Sankey, C. Yang, B. M. Zwickl, A. M. Jayich, and J. G. E. Harris. *Nat. Phys.*, 6(9):707–712, 2010.
- [30] Itamar Katz, Alex Retzker, Raphael Straub, and Ron Lifshitz. Phys. Rev. Lett., 99(4):040404, 2007.

- [31] Itamar Katz, Ron Lifshitz, Alex Retzker, and Raphael Straub. *New J. Phys.*, 10(12):125023, 2008.
- [32] Berihu Teklu, Alessandro Ferraro, Mauro Paternostro, and Matteo G. A. Paris. EPJ Quantum Technol., 2(16):10, 2015.
- [33] Francesco Albarelli, Alessandro Ferraro, Mauro Paternostro, and Matteo G. A. Paris. *Phys. Rev. A*, 93(3):032112, 2016.
- [34] A. S. Holevo. Probabilistic and Statistical Aspects of Quantum Theory. Springer Science & Business Media, 2011.
- [35] C. W. Helstrom. J. Stat. Phys., 1(2):231–252, 1969.
- [36] M. G. A. Paris. Int. J. Quantum Inf., 7(supp01):125-137, 2009.
- [37] F. Albarelli, M. Barbieri, M. G. Genoni, and I. Gianani. *Phys. Lett. A*, 384(12):126311, 2020.
- [38] Abdelatif Chabane, Sidali Mohammdi, Abdelhakim Gharbi, and Matteo G. A. Paris. Int. J. Quantum Inf., 23(5):2550004, 2025.
- [39] Philip M Morse. Phys. Rev., 34(1):57–64, 1929.
- [40] M Razavy. Am. J. Phys., 48(4):285-288, 1980.
- [41] Eiko Matsushita and Takeo Matsubara. Prog. Theor. Exp. Phys., 67(1):1–19, 1982.
- [42] G N Robertson and M C Lawrence. J. Phys. C. Solid State Phys., 14(31):4559–4574, 1981.
- [43] H Konwent. Phys. Lett. A, 118(9):467-470, 1986.
- [44] Henryk Konwent, Pawel Machnikowski, Piotr Magnuszewski, and Andrzej Radosz. J. Phys. A: Math. Gen., 31(37):7541, 1998.
- [45] B Zaslavskii and VV Ul'yanov. Zh. Eksp. Teor. Fiz, 87:1724– 1733, 1984.
- [46] SV Goryainov. Physica B, 407(21):4233-4237, 2012.
- [47] Timothy D Davis and Ralph E Christoffersen. *Chem. Phys. Lett.*, 20(4):317–322, 1973.
- [48] Michael Berblinger and Christoph Schlier. *Chem. Phys. Lett.*, 145(4):299–304, 1988.
- [49] Barry K Carpenter, Gregory S Ezra, Stavros C Farantos, Zeb C Kramer, and Stephen Wiggins. Regul. Chaot. Dyn., 23:60–79, 2018
- [50] BA Pettitt. J. Chem. Educ., 75(9):1170, 1998.
- [51] H Konwent, P Machnikowski, and A Radosz. J. Phys. A: Math. Gen., 28(13):3757, 1995.
- [52] Zhenhua Li. Quantum resonant beats and revivals in the morse oscillators and rotors. University of Arkansas, 2013.
- [53] Alexander G Ushveridze. Quasi-exactly solvable models in quantum mechanics. CRC Press, 1994.
- [54] Alvason Zhenhua Li and William G. Harter. Quantum revivals of morse oscillators and farey-ford geometry. *Chemical Physics Letters*, 633:208–213, 2015.
- [55] Matteo GA Paris, Marco G Genoni, Nathan Shammah, and Berihu Teklu. *Phys. Rev. A*, 90(1):012104, 2014.
- [56] Marco G Genoni, Matteo GA Paris, and Konrad Banaszek. *Phys. Rev. A*, 78(6):060303, 2008.
- [57] Marco G Genoni and Matteo GA Paris. Phys. Rev. A, 82(5):052341, 2010.
- [58] Eugene Wigner. Phys. Rev., 40(5):749-759, 1932.
- [59] K. E. Cahill and R. J. Glauber. Phys. Rev., 177(5):1882–1902, 1969
- [60] R. F. O'Connell, Lipo Wang, and H. A. Williams. *Phys. Rev. A*, 30(5):2187–2192, 1984.
- [61] Robin L Hudson. Reports on Mathematical Physics, 6(2):249– 252, 1974.
- [62] Anatole Kenfack and Karol Życzkowski. *J. Opt. B: Quantum Semiclass. Opt.*, 6(10):396–404, 2004.
- [63] Mattia Walschaers. PRX quantum, 2(3):030204, 2021.
- [64] Milton Abramowitz and Irene A Stegun. Handbook of mathematical functions with formulas, graphs, and mathematical tables, volume 55. US Government printing office, 1972.
- [65] Charles B Balogh. SIAM J. Appl. Math., 15(5):1315-1323, 1967.
- [66] T Mark Dunster. SIAM J. Math. Anal., 21(4):995–1018, 1990.

- [67] Amparo Gil, Javier Segura, and Nico M Temme. J. Comput. Appl. Math.., 153(1-2):225–234, 2003.
- [68] Andrew R Booker, Andreas Strömbergsson, and Holger Then. LMS J. Comput. Math., 16:78–108, 2013.
- [69] Y Aharonov, D Falkoff, E Lerner, and H Pendleton. Ann. Phys., 39(3):498–512, 1966.
- [70] M. S. Kim, W. Son, V. Bužek, and P. L. Knight. *Phys. Rev. A*, 65(3):032323, 2002.
- [71] János K. Asbóth, John Calsamiglia, and Helmut Ritsch. *Phys. Rev. Lett.*, 94(17):173602, 2005.
- [72] Josef Kadlec, Karol Bartkiewicz, Antonín Černoch, Karel Lemr, and Adam Miranowicz. Phys. Rev. A, 110(2):023720, 2024.
- [73] Adam Miranowicz, Karol Bartkiewicz, Neill Lambert, Yueh-Nan Chen, and Franco Nori. Phys. Rev. A, 92(6):062314, 2015.
- [74] Alex Monras and Matteo G. A. Paris. *Phys. Rev. Lett.*, 98(16):160401, 2007.
- [75] U. Dorner, R. Demkowicz-Dobrzanski, B. J. Smith, J. S. Lundeen, W. Wasilewski, K. Banaszek, and I. A. Walmsley. *Phys. Rev. Lett.*, 102(4):040403, 2009.
- [76] Giorgio Brida, Ivo Pietro Degiovanni, Angela Florio, Marco Genovese, Paolo Giorda, Alice Meda, Matteo G. A. Paris, and Alexander Shurupov. *Phys. Rev. Lett.*, 104(10):100501, 2010.
- [77] Davide Brivio, Simone Cialdi, Stefano Vezzoli, Berihu Teklu Gebrehiwot, Marco G. Genoni, Stefano Olivares, and Matteo G. A. Paris. *Phys. Rev. A*, 81(1):012305, 2010.
- [78] Carmen Invernizzi, Matteo G. A. Paris, and Stefano Pirandola. Phys. Rev. A, 84(2):022334, 2011.
- [79] Marco G. Genoni, Stefano Olivares, and Matteo G. A. Paris. *Phys. Rev. Lett.*, 106(15):153603, 2011.
- [80] Mankei Tsang, Howard M. Wiseman, and Carlton M. Caves. Phys. Rev. Lett., 106(9):090401, 2011.
- [81] Marco G. Genoni, Stefano Olivares, Davide Brivio, Simone

- Cialdi, Daniele Cipriani, Alberto Santamato, Stefano Vezzoli, and Matteo G. A. Paris. *Phys. Rev. A*, 85(4):043817, 2012.
- [82] M. G. Genoni, M. G. A. Paris, G. Adesso, H. Nha, P. L. Knight, and M. S. Kim. *Phys. Rev. A*, 87(1):012107, 2013.
- [83] O. Pinel, P. Jian, N. Treps, C. Fabre, and D. Braun. *Phys. Rev. A*, 88(4):040102, 2013.
- [84] Alessandro Candeloro, Sholeh Razavian, Matteo Piccolini, Berihu Teklu, Stefano Olivares, and Matteo G. A. Paris. *Entropy*, 23(10):1353, 2021.
- [85] Muhammad Asjad, Berihu Teklu, and Matteo GA Paris. *Physical Review Research*, 5(1):013185, 2023.
- [86] Simone Cavazzoni, Berihu Teklu, and Matteo G. A. Paris, 2025.
- [87] Abdelatif Chabane, Sidali Mohammdi, Abdelhakim Gharbi, and Matteo G. A. Paris. Int. J. Quantum Inf., 23(05):2550004, 2025.
- [88] Sergio Boixo, Steven T. Flammia, Carlton M. Caves, and JM Geremia. Phys. Rev. Lett., 98(9):090401, 2007.
- [89] Paolo Zanardi, Matteo G. A. Paris, and Lorenzo Campos Venuti. Phys. Rev. A, 78(4):042105, 2008.
- [90] Tyler Volkoff and Giri Gopalan. J. Phys. A: Math. Theor., 58(41):41LT01, 2025.
- [91] I. Sh. Averbukh and N. F. Perelman. Phys. Lett. A, 139(9):449–453, 1989.
- [92] R. W. Robinett. Phys. Rep., 392:1–119, 2004.
- [93] H. Stapelfeldt and T. Seideman. Rev. Mod. Phys., 75:543–557, 2003
- [94] Christiane P. Koch, Mikhail Lemeshko, and Dominique Sugny. *Rev. Mod. Phys.*, 91:035005, 2019.
- [95] D. DeMille. Phys. Rev. Lett., 88:067901, 2002.
- [96] M. V. Berry and S. Klein. J. Mod. Opt., 43(10):2139–2164, 1996
- [97] René L Schilling. Measures, integrals and martingales. Cambridge University Press, 2017.